CrossMark

RESEARCH ARTICLE

Quantitative effects of acquisition duration and temporal resolution on the measurement accuracy of prostate dynamic contrast-enhanced MRI data: a phantom study

Silvin Paul Knight[1] · **Jacinta Elizabeth Browne**[2] · **James Frances Mary Meaney**[1] ·
Andrew John Fagan[1]

Abstract

Objectives The aim of this study was to investigate the effect of the temporal resolution (T_{res}) and acquisition duration (AD) on the measurement accuracy of contrast concentration–time curves (CTCs), and derived phenomenological and pharmacokinetic parameter values, in a dynamic contrast-enhanced MRI experiment using a novel phantom test device.

Materials and methods 'Ground truth' CTCs were established using a highly precise optical imaging system. These precisely known CTCs were produced in an anthropomorphic environment, which mimicked the male pelvic region, and presented to the MRI scanner for measurement. The T_{res} was varied in the range [2–24.4 s] and the AD in the range [30–600 s], and the effects on the measurement accuracy were quantified.

Results For *wash-in* parameter measurements, large underestimation errors (up to 40%) were found using T_{res} values ≥16.3 s; however, the measured *wash-out* rate did not vary greatly across all T_{res} values tested. Errors in derived K^{trans} and v_e values were below 14 and 12% for acquisitions with {$T_{res} \leq 8.1$ s, AD ≥ 360 s} and {$T_{res} \leq 16.3$ s, AD ≥ 360 s}, respectively, but increased dramatically outside these ranges.

Conclusions Errors in measured *wash-in*, *wash-out*, K^{trans}, and v_e parameters were minimised using $T_{res} \leq 8.1$ s and AD ≥ 360 s, with large errors recorded outside of this range.

Introduction

In dynamic contrast-enhanced magnetic resonance imaging (DCE-MRI) a series of consecutive T_1-weighted MR images are acquired after the administration of a bolus of paramagnetic gadolinium-based contrast agent (CA). As the bolus of CA arrives at the tissue of interest it modifies the inherent relaxation rates of the protons in that region, effecting a change in the measured signal intensity. By collecting a consecutive series of images, a signal intensity-time curve is produced at each imaging voxel, from which contrast concentration–time curves (CTCs) can be derived. Phenomenological parameters, such as the *wash-in* and *wash-out* rates can be calculated from the CTCs, and since the shape of the CTCs is related to the perfusion conditions of the tissue being imaged, pharmacokinetic (PK) modelling can also be used to estimate physiological parameters, such as the volume transfer coefficient (K^{trans}) [min^{-1}] and extravascular-extracellular volume fraction (v_e), providing quantitative information related to the vascular properties of the tissue.

Prostate cancer (PCa) is known to have increased vascular density, permeability, and interstitial fluid volume compared with healthy prostate tissue, leading to tumorous tissue exhibiting earlier enhancement and higher washout,

✉ Andrew John Fagan
  faganan@tcd.ie

[1] School of Medicine, Trinity College University of Dublin / National Centre for Advanced Medical Imaging (CAMI), St James's Hospital, Dublin 8, Ireland

[2] School of Physics and Medical Ultrasound Physics and Technology Group, Centre of Industrial Engineering Optics, FOCAS, Dublin Institute of Technology, Dublin 8, Ireland

with higher-grade tumours tending to have higher rate constants [1, 2]. Since these tissue properties are known to vary significantly between malignant and benign prostate tissues [3], phenomenological curve-shape analysis and PK modelling of DCE-MRI data shows great promise as a potential non-invasive gold standard imaging technique for PCa detection [1], localisation [4, 5], and grading [2, 6]. However, the widespread acceptance of DCE-MRI has been hindered by discrepancies in the published results, mainly as a result of methodological differences between studies. The quality of MR-derived parameters is known to be influenced by the experimental settings governing the data acquisition and hence the measurements [7], with adequate acquisition duration (AD; the overall length of time that the CTC is acquired for from the start of the CA enhancement) and temporal resolution (T_{res}; the time-spacing between subsequent image volumes) being required for accurate PK model fitting [8, 9]. For optimal parameter estimation, the T_{res} should be sufficiently high to adequately capture the rapidly changing features of the CTC (i.e. the wash-in phase) and the AD should be long enough to include the slowly changing features (i.e. wash-out phase). Additionally, long ADs can introduce motion artefacts in patient imaging, which can be an additional source of measurement errors [8], while conversely, inadequate ADs can lead to underestimation of perfusion parameters [9]. Considering the range of DCE-MRI acquisition and analysis protocols reported in the literature, and the large variability in data derived from these varied approaches, it is apparent that a reliable 'gold standard' method is required for determining the measurement accuracy of the CTCs, as well as derived parameters, with errors calculated against known ground truth values [9–11].

Previous attempts to investigate DCE-MRI measurements have used model phantom systems to physically mimic permeable microvasculature [12, 13]. However, in none of these systems were the 'true' or 'ground truth' values known, where the 'ground truth values' in this context refer to an accurate and precise knowledge of the actual CTCs within the object being scanned. Indeed, only when such ground truth CTCs are known can the accuracy of a DCE measurement be determined. Additionally, none of these previous designs have allowed for MR measurements to be made in an environment which realistically challenges the prostate DCE-MR imaging protocol by closely mimicking conditions observed in vivo. Theoretical approaches have also been used to investigate the effects of T_{res} and AD on PK parameter measurements [9, 14]; however, although beneficial in the planning of MRI protocols, a purely theoretical approach does not allow for the full assessment of the MR scanner's ability to accurately measure known reference CTCs using a particular protocol. Other studies have used retrospectively resampled patient prostate data to

investigate the effects of reduced AD and T_{res} [10, 15, 16], but, again, the ground truth values are not known and hence the measurement accuracy of the resampled data (or even the fully sampled data) cannot be assessed.

Previous DCE-MRI studies have reported using a wide range of both T_{res} (~2–30 s) and AD (~90–760 s) values for the acquisition of data in the prostate [17–20]. The aim of the present work was to use a recently developed novel DCE-MRI prostate phantom test device, in which MR-measured CTCs could be compared with precisely known ground truth values [21], to quantitatively investigate the effects of T_{res} and AD on the accuracy of MR-measured CTCs, as well as phenomenological and PK parameters derived from these CTCs, across a range of T_{res} and AD values used in previously published prostate DCE-MRI studies.

Materials and methods

MRI measurements

DCE-MRI data were acquired using a 3T scanner (Achieva TX, Philips, The Netherlands) and a 32-channel phased array detector coil. A 3D spoiled gradient echo imaging sequence with multi-transmit was used, with the following scan parameters: repetition time (TR) = 4.3 ms; echo time (TE) = 1.4 ms; flip angle = 10°; FOV = 224 × 224 × 80 mm³; spatial resolution = 1 × 1 × 4 mm³; no parallel imaging (R-factor); and number of signal averages (NSA) = 1; resulting in a T_{res} of 8.1 s. This protocol was then modified by applying parallel imaging to produce protocols with T_{res} values of 2, 3.8, and 5.3 s [R-factor (AP/FH) = 2/2, 1.8/1.3, and 1.3/1.3, respectively]. Additionally, the NSA was increased to produce protocols with T_{res} = 16.3 and 24.4 s (NSA = 2 and 3, respectively). This resulted in six scanning protocols, with T_{res} values across a range which was in line with those used in previously published prostate DCE-MRI studies. Each 720-s experimental run consisted of at least 5 dynamic scans measured at the baseline CA concentration and with the remaining dynamics measured for a further 600 s (i.e. AD = 600 s). The fully sampled MR data thus acquired was then retrospectively truncated to produce sub-sets of data at AD = 480, 360, 240, 180, 120, 60, and 30 s.

Contrast concentration–time curves (CTCs)

'Healthy' and 'tumour' tissue-mimicking CTCs were generated using the standard Tofts model [22], a model arterial input function (AIF) [23], and input PK parameters taken from representative published patient data [K^{trans} = 0.14 ('healthy') and 0.36 ('tumour'); v_e = 0.47 ('healthy' and

0.55 ('tumour')] [18, 24]. The CTCs consisted of 120 s of baseline data, followed by a 600-s physiological CTC shape mimicking those typically observed in healthy or tumorous tissue. Ground truth CTCs were established from repeated measurements made using a highly precise ($\pm 0.4\%$), high spatiotemporal-resolution optical imaging system [21]. Concordance correlation coefficient (CCC) analysis was performed on the repeat optical measurements, using Statistical Package for the Social Sciences (SPSS; v.22, IBM Corp, USA), with high reproducibility calculated between repeat optical experimental CTC runs (CCC = 0.992, 95% confidence intervals = {0.990, 0.993}).

Phantom

The anthropomorphically shaped phantom device used herein allowed for the simultaneous production of two distinct CTCs, for which ground truth values were known a priori, within an environment which closely mimics the male pelvic region. The CTCs were produced by means of a custom-built, computer-controlled, four-pump flow system, by alternating the instantaneous volume of solutions pumped from two reservoirs, each containing different concentrations (0.15 and 1.5 mM) of a contrast agent (Multihance, Bracco, USA). The mixing of these solutions in turn created the desired concentration of the CA at a particular time-point, giving rise to the desired CTC shapes, which was subsequently measured within two 'measurement chambers' located inside a prostate-mimicking region of the anthropomorphic phantom. The measurement chambers were designed to ensure an optimally uniform distribution of fluids at each instant of time at the low flow rate used (1.5 ml s^{-1}), thereby avoiding any mixing bias within the regions of interest placed inside each measurement chamber in the MR images.

The phantom system was calibrated using a custom-built, high-spatiotemporal resolution optical imaging system, which was set up using the same tubing configuration and lengths as used for the main phantom device, with two pumps producing CTCs within a single measurement chamber, set within a custom-built, light-sealed enclosure. A highly-stable endoscopic light source (Fujinon Eve Σ400, Fujifilm Corp, Japan) was used in conjunction with a high-resolution CMOS camera (Canon 50D, Canon Inc, Japan) with a 4752 × 3168 array for detection (4 × 4 µm^2 pixels; T_{res} = 1 s). The signal intensity was modified over time to produce the required CTCs by adjusting the concentration of black dye (used as a CA surrogate in the system) in the measurement chamber, with precise concentrations being subsequently calculated using a calibration method. Further details of this novel phantom device and calibration system can be found in Ref. [21].

Data analysis

The AIF used in this present work for the analysis of all optical and MR data was generated using code developed in MatLab (R2015b, MathWorks, USA) at temporal resolutions matching those used in the optical and MR studies [23]. CCC values were calculated between the MR-measured and ground truth CTCs (AD = 600 s); the CTCs were temporally aligned (MR-measured and ground truth), and ground truth CTC temporally resampled to match the MR data points prior to analysis. CCC values were used as a metric for both the precision (ρ, the Pearson correlation coefficient, a measure of the degree of scatter) and accuracy (C_b, a bias correction factor, the degree of systematic location and scale shifts) of the full CTC measurements [25]. The *wash-in* (the maximum slope between the time of onset of contrast inflow and the time of peak intensity) and *wash-out* (the maximum slope of the late-wash phase of the curve) rates [2] were calculated from the CTCs at two manually selected regions of interest (ROIs), each containing 26 voxels and set within the respective measurement chamber (voxel-wise analysis), as illustrated in Fig. 1. Voxel-wise PK modelling using the standard Tofts model was also performed at the same ROIs using the *DCEMRI. jl* toolkit [26]. *Wash-in*, *wash-out*, K^{trans}, and v_e values were derived from the MR-measured CTCs and compared with the ground truth values (derived from the optically measured CTCs), with the percentage differences calculated.

Signal to noise ratio (SNR) values were calculated in the same ROIs used for the CTC analysis using a 'difference method' [27], based on the evaluation of a difference between two repeated acquisitions at baseline concentration, given as

$$\text{SNR}_{\text{diff}}(b_1, b_2) = \frac{\frac{1}{2}\bar{S}_{\mathbf{r}\in\text{ROI}}(S_N(\mathbf{r}, b_1) + S_N(\mathbf{r}, b_2))}{\frac{1}{\sqrt{2}}\sigma_{\mathbf{r}\in\text{ROI}}(S_N(\mathbf{r}, b_1) - S_N(\mathbf{r}, b_2))}, \quad (1)$$

where $\bar{S}_{\mathbf{r}\in\text{ROI}}$ is the mean signal value and $\sigma_{\mathbf{r}\in\text{ROI}}$ is the standard deviation, for calculations performed at each imaging voxel ($\mathbf{r}$) in the ROI, and $S_N(\mathbf{r}, b_n)$ is the signal at each imaging voxel in the ROI for each respective baseline measurement (b_1 and b_2).

Results

Figure 2 shows representative dynamic images taken from the MR data at the 'tumour' CTC peak at each of the T_{res} values tested, along with SNR values derived from the DCE-MRI data; SNR increased as the T_{res} value was increased. Furthermore, this increase in SNR was evident in the MR-measured CTCs as a decrease in signal variation across the ROIs, resulting in a reduction in

Fig. 1 Representative T_2-weighted (**a**) axial and (**b**) coronal scans of the phantom during peak enhancement within the 'prostate' region. The *white box* in (**a**) *outlines* the region shown in (**c**). **c** Pharmacokinetic parameter map (K^{trans}) showing the ROIs placed within the measurement chambers which were used to measure the healthy (ROI 1) and tumour (ROI 2) parameter values
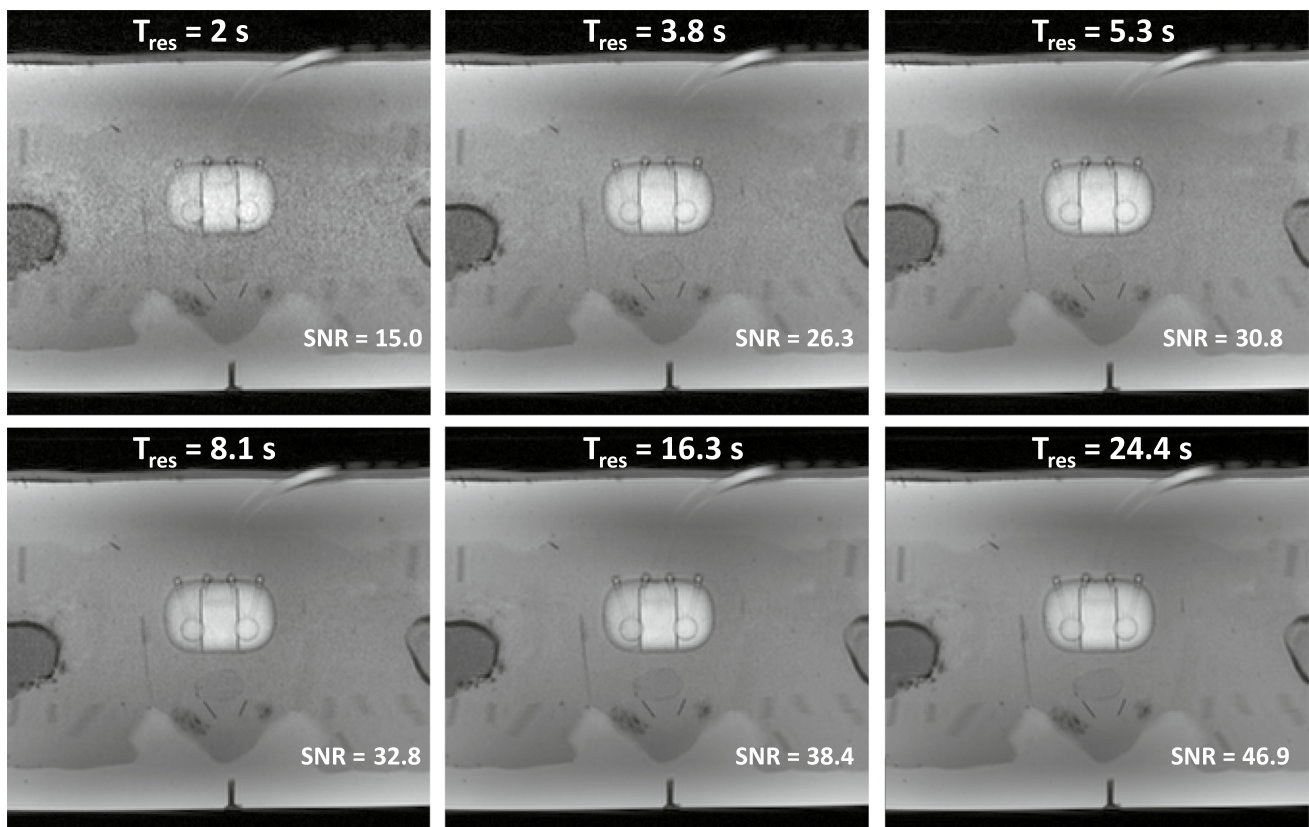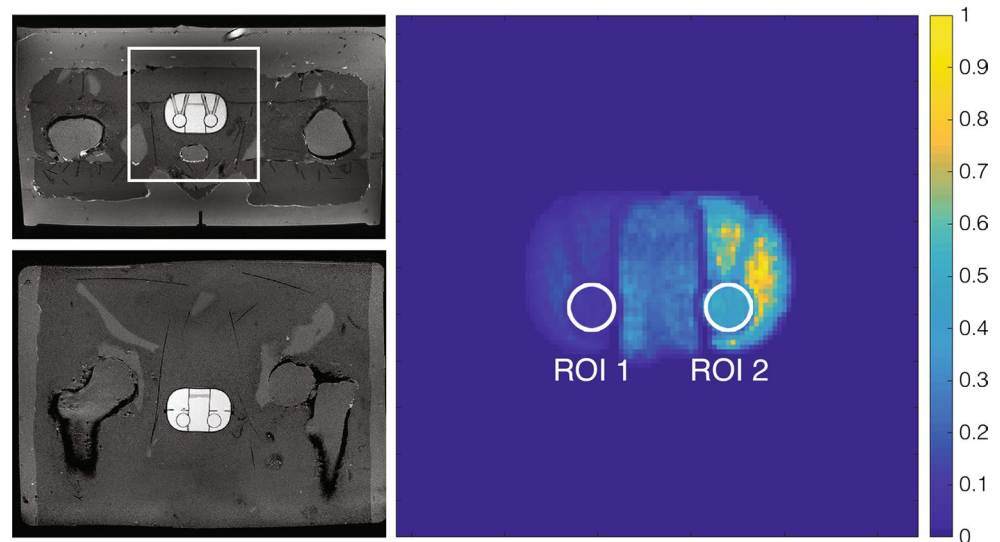

Fig. 2 Representative dynamic images taken from the MR-data at the CTC peak (tumour) at each of the T_{res} values tested. SNR values derived from the DCE-MRI data are also presented. (SNR results presented herein should be treated as relative, for the purpose of highlighting relative behavioural trends in the data)

the calculated uncertainties, as shown in Fig. 3. Figure 3 also shows an underestimation in the measurement of the 'tumour' CTC peak using protocols with $T_{res} < 8.1$ s, as well as an overestimation of the wash-out phase of the tumour CTC for all protocols tested. Ground truth CTCs are shown in Fig. 3 as solid red ('tumour') and blue ('healthy') lines.

Figure 4 shows the correlation plots comparing the MR-measured and ground truth CTCs, as well as the CCC values with 95% confidence intervals. Inaccuracies in the
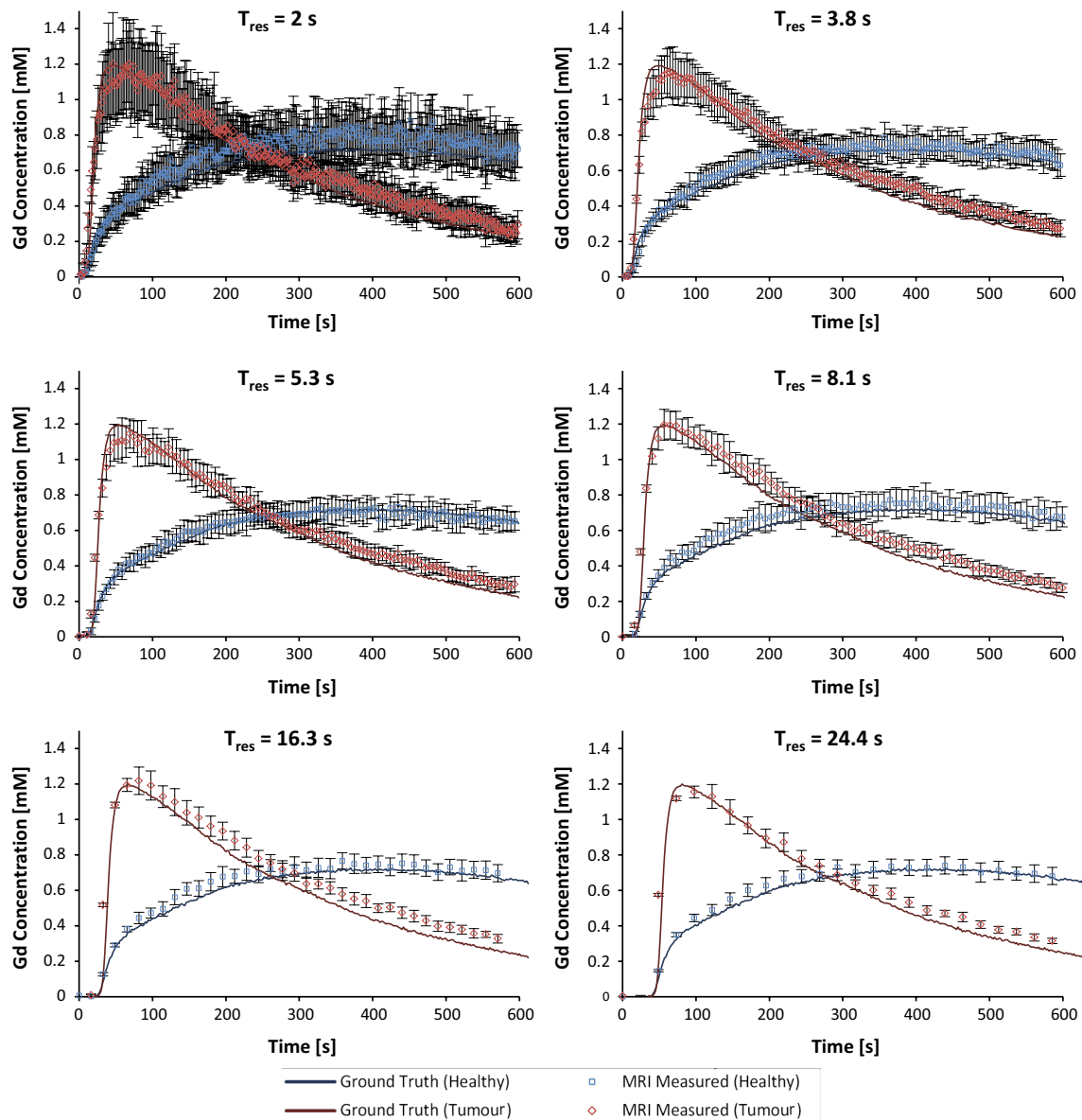
Fig. 3 Graphs showing the MR-measured CTCs at different T_{res} values, with *error bars* derived from the standard deviation across the ROI. Ground truth CTCs are also shown as *solid lines*

measurement of the wash-in phase of the 'tumour' CTC were evident as outlying data points, when using T_{res} values ≤8.1 s. Using the fastest protocol ($T_{res} = 2$ s), there was an overestimation of the MR-measured healthy CTC at higher concentration (>0.3 mM), and these measurement inaccuracies were also apparent in the relatively low CCC value of 0.906 (95% CI = {0.889, 0.920}). There was a general trend for higher CCC values as T_{res} was increased.

Errors in the measured *wash-in* and *wash-out* parameter values are given in Fig. 5. For the measurement of the *wash-in*, despite the fact that the standard deviation across the ROI was reduced with increased T_{res} (as evidenced by a reduction in the size of the error bars),

large underestimation errors (up to 40%) were measured using protocols with T_{res} values ≥16.3 s. Errors in the measurement of the 'tumour' CTC *wash-out* did not vary greatly across all T_{res} values tested, with all errors <15%; however, there was large variation in the *wash-out* values calculated across the ROI for the 'healthy' CTCs (as evidenced by the large uncertainties of up to ±65%, see Fig. 5), indicating that all protocols struggled to measure this portion of the 'healthy' CTC accurately.

Figures 6 and 7 present the percentage errors in the PK parameter values derived from the DCE-MRI data at different T_{res} and AD values using the standard Tofts model.
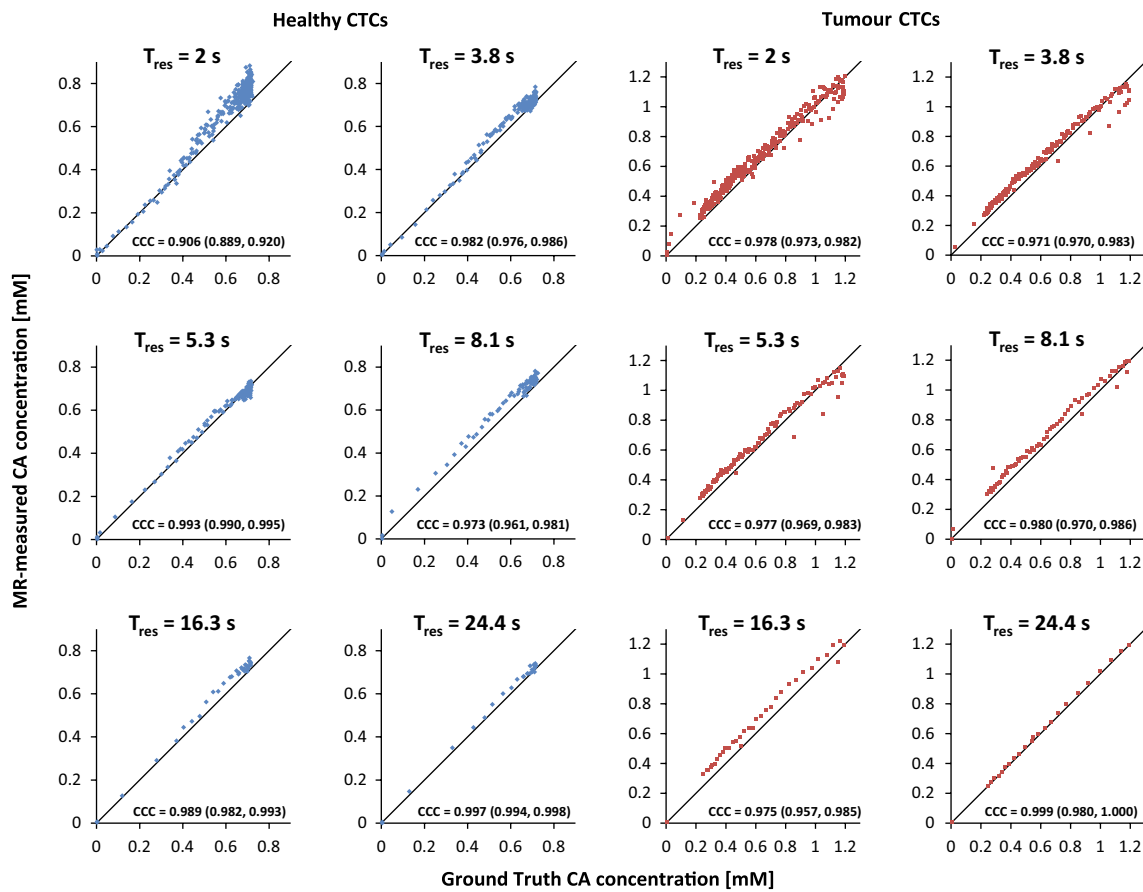
Fig. 4 Correlation plots of the MR-measured versus ground truth CTCs for full 600-s CTC measurements. The *diagonal line* indicates equality, with divergence from this *line* indicating discrepancies between the MR-measured and ground truth values. The CCC values are also shown, along with their 95% confidence intervals
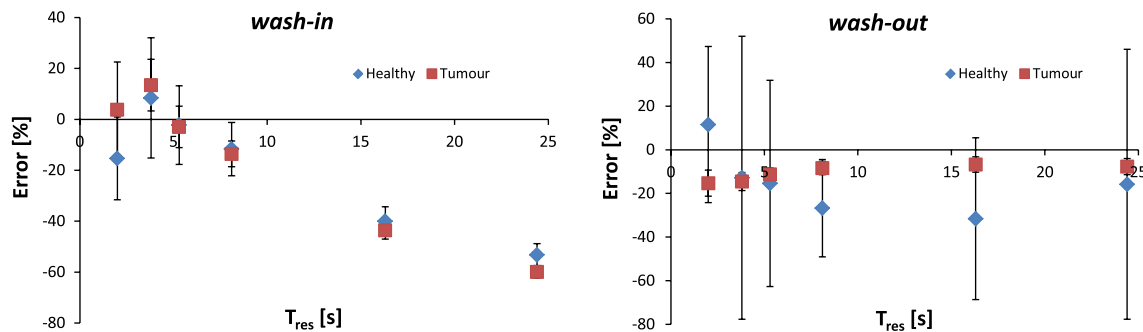

Fig. 5 Percentage errors in *wash-in* and *wash-out* parameter values derived from the DCE-MRI data at different temporal resolutions using the standard Tofts model. *Error bars* are derived from the standard deviation of the data

K^{trans} and v_e values derived from the MR data differed from the ground truth values by up to 230 and 98%, respectively. Errors of <14% were found for all MR-measurements of K^{trans} made at AD ≥360 s and T_{res} ≤ 8.1 s. The 24.4-s protocol was the least accurate in the measurement of K^{trans}, with errors of up to 172% using the full 600-s acquisition, and these errors increased as the AD was reduced, as

shown in Fig. 6 (bottom-right graph). For the measurement of v_e, errors of <12% were measured at T_{res} ≤16.3 s, with AD ≥360 s. As with the measurement of K^{trans}, the greatest errors in the measurement of v_e were observed in data measured at T_{res} = 24.4 s. The lowest overall errors (<10%) in the measurement of both 'tumour' and 'healthy' K^{trans} and v_e values occurred using: T_{res} = 2 s, with AD ≥360 s.
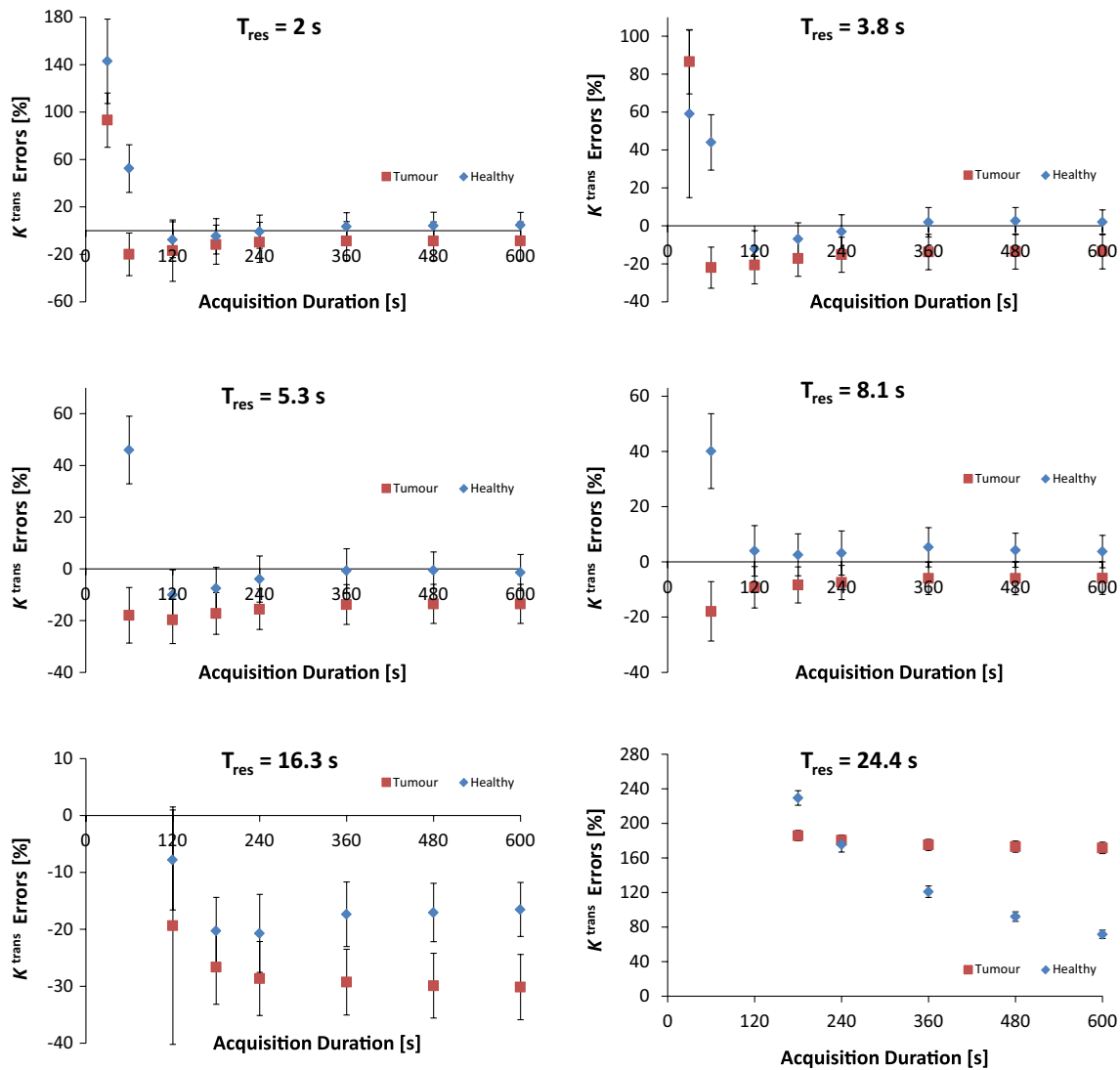
Fig. 6 Percentage errors in K^{trans} values derived from the DCE-MRI data at different temporal resolutions and acquisition lengths using the standard Tofts model. *Error bars* are derived from the standard deviation of the data

Discussion

The absence of a robust validation method has contributed to a lack of standardisation in the way that DCE-MRI is performed, hindering its full clinical implementation and rendering comparisons between published studies difficult [8]. As a consequence, the published literature is replete with many different DCE acquisition and analysis protocols, resulting in inconsistencies in the reported data. It is clear that a consensus needs to be reached regarding the optimal data acquisition and analysis methodology to use, so that consistent evidence-based data can be accumulated. The current study demonstrates the trade-offs which arise from modifications of a prostate DCE acquisition protocol involving two of the most widely varied acquisition parameters: temporal resolution

and AD. This was possible through the use of a novel phantom device wherein precisely known ground truth CTCs could be repeatedly produced and presented to the MRI scanner for measurement, and hence the accuracy of the measured CTCs; additionally, phenomenological (*wash-in* and *wash-out*) and PK (K^{trans} and v_e) parameter values derived from these CTCs could be determined.

The data presented herein for a standard 3D spoiled gradient-recalled echo DCE imaging sequence (with a T_{res} of 8.1 s) demonstrates that non-negligible errors in *wash-in*, *wash-out*, K^{trans}, and v_e parameters occur for both tumour and healthy tissue-like regions. Similar, if not larger, errors can be expected with rapidly accelerated techniques such as parallel imaging and compressed sensing (used to reduce T_{res} values to facilitate more complex PK modelling), where decreases in SNR will invariably
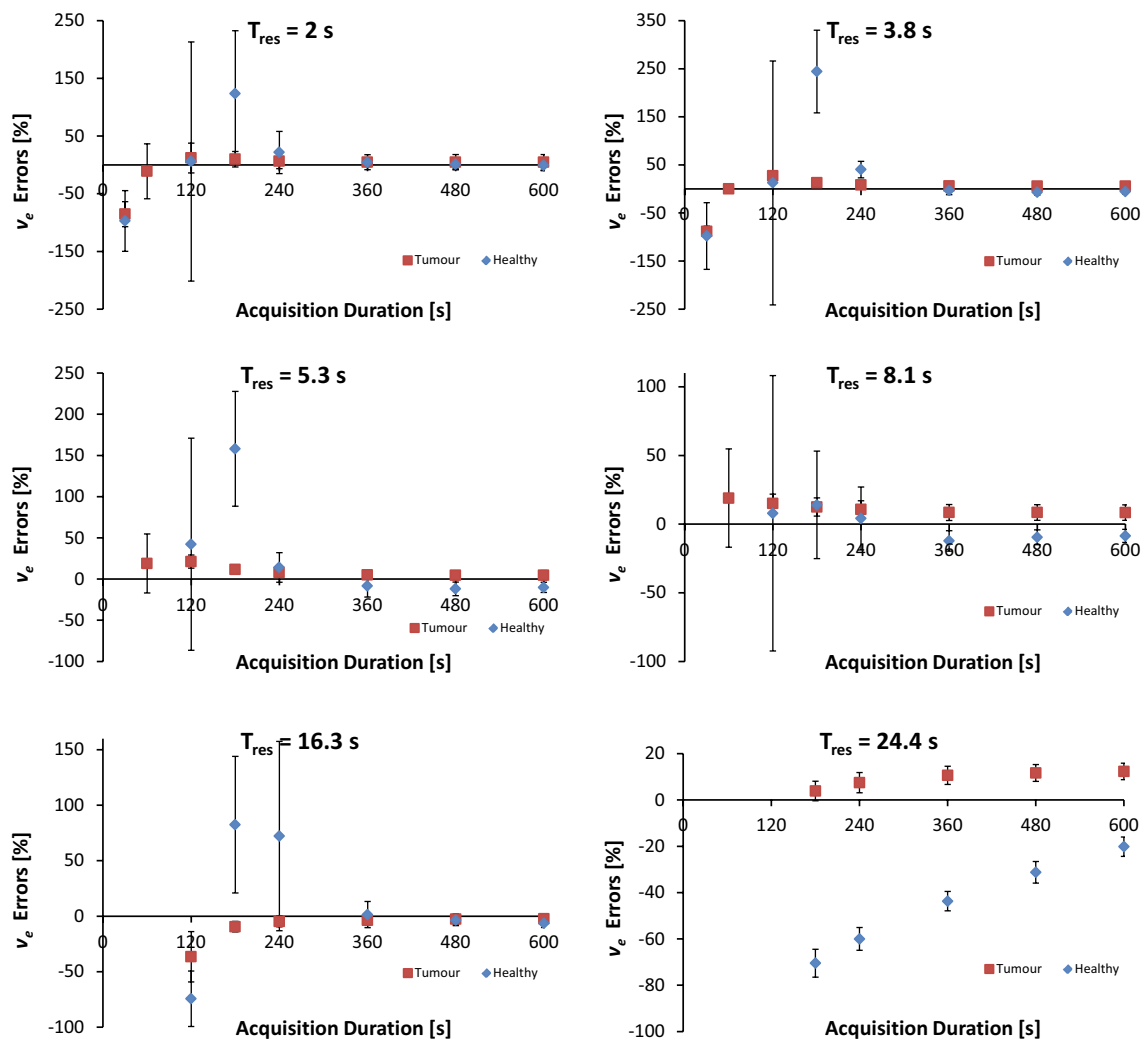
Fig. 7 Percentage errors in v_e values derived from the DCE-MRI data at different temporal resolutions and acquisition lengths using the standard Tofts model. *Error bars* are derived from the standard deviation of the data

occur [28]. The measured CCC values increased with increasing T_{res}, indicating greater precision and accuracy in the point-by-point measurement of the CTCs; however, further parametric analysis of the CTCs showed that the reduced number of data points, resulting from larger T_{res} values, hindered the accurate measurement of certain important curve-shape features. Prior studies have reported that model-free phenomenological parameters, such as the *wash-in* and *wash-out* rates, increase the specificity and sensitivity for PCa detection compared with other diagnostic techniques, even when using T_{res} values as high as 30 s [5, 29]. However, the actual *wash-in* and *wash-out* rates were not known in these studies, but rather a relative comparison of the measured rate values across the prostate area was performed. The current work demonstrates that a T_{res} value ≤8.1 s is required for accurate measurement of the absolute *wash-in* rate.

Conflicting data has been published in the literature regarding the effect of T_{res} on PK parameter measurements. For example, in a theoretical simulation study, Aerts et al. reported that the T_{res} requirements were strongly related to the actual PK parameter values being measured, with lower T_{res} values required for the precise measurement of higher K^{trans} values [9]. The physical data from the current study corroborates these theoretical findings, with up to 50% greater precision in the measurement of the lower (healthy) versus higher (tumour) K^{trans} values observed, as well as two to ten times higher accuracy in the measured K^{trans} values (using T_{res} of ≤8.1 s). For higher T_{res} values, the K^{trans} accuracy decreased markedly due to inadequate sampling of the *wash-in* portion of the curves. T_{res} had less effect on the accuracy of v_e measurements, with errors found to be fairly consistent at up to approximately 10% for T_{res} values of ≤16.3 s (AD = 600 s), increasing moderately

to approximately 20% using $T_{res} = 24.4$ s; in this case, a variation in the number of sampling points due to modified T_{res} did not cause a major hindrance in the measurement of the final peak value of the CTCs, a key component for the accurate measurement of v_e. This is in line with the recent findings of Ginsburg et al. where it was reported that the effect of temporal resolution was different for estimates of K^{trans} than for v_e [10]. Another recent study reported no significant effect of varying T_{res} on PK parameter values [16]; however, T_{res} values of 5–30 s in this study were obtained by a retrospective resampling of the original $T_{res} = 5$ s data set, with a relative comparison among datasets used to explore any PK parameter changes, without knowledge of the ground truth values.

Reported AD values have also varied widely in published DCE-MRI studies, again with conflicting results presented. In one theoretical study, AD values greater than 420 s were found to offer no improvement in PK parameter estimation for T_{res} values of less than 10 s, whereas below 420 s, the precision in the measurement of higher K^{trans} values was found to decrease [9]. Conversely, another study investigated the effect of retrospectively reducing the AD of patient prostate DCE data on the measured K^{trans} and v_e values, and reported no statistical difference using acquisition lengths as short as 150 s in the former and 50 s for the latter [15]. However, these results were based on a 'full acquisition' length of only 250 s, against which the PK parameter values measured from retrospectively reduced data sets (AD = 50, 100, 150, and 200 s) were compared in a relative sense, and hence any potential CTC truncation effects (particularly on v_e measurements) are unknown. In the current study, large errors in 'healthy' v_e values were measured for AD values ≤ 240 s, which may be attributed to the appearance of the peak in the 'healthy' CTC at approximately 345 s: the v_e parameter estimation from PK model fitting is critically dependent on the CTC reaching a clearly identifiable peak, with some degree of subsequent wash-out, in order for the model fit to produce an accurate v_e value. For instance, this explains why, in the current study for the 'tumour' CTC used (where the peak of the CTC appeared at approximately 35 s), a reasonably good v_e measurement accuracy was maintained with AD values as low as 180 s (<13% error using all T_{res} values tested). Thus, the findings in [15] that ADs as low as 50 s did not significantly change the measured v_e values may only be valid for certain CTC shapes with peaks occurring at early time points (for example, as found typically in malignant tumours with fast wash-in/wash-out profiles). Indeed, this critical dependence on an adequate AD for the accurate measurement of v_e for different tissue/tumour types may explain the wide discrepancy in published v_e values and the consequent perceived lack of diagnostic sensitivity and specificity to

PCa detection. One such example is provided by a study by Chen et al. which reported no significant difference for v_e values measured in tumour verses healthy prostate tissue which, in the light of the present study's results, may have been strongly influenced by the short 120-s AD used for the measurements [6]. On the other hand, the authors did report that the measured K^{trans} values were significantly higher in tumour tissue compared with healthy tissue, even at the short 120-s AD [6], and this was also seen in the present work where the AD was not found to exert a strong influence on the accuracy of K^{trans} measurements for AD values ≥ 120 s and for $T_{res} \leq 8.1$ s. Considering the critical dependence of the accuracy of the K^{trans} parameter estimation on the initial wash-in slope of the CTC, this result is perhaps not surprising. Indeed, the results presented herein, along with those of those of certain previous patient studies, suggest that acquisition times as low as 120 s could be justified if K^{trans} is the sole object of any PK modelling exercise. On the other hand, if v_e is also to be measured, longer ADs are required. In establishing an optimum AD, clinical studies will also need to consider the potential detrimental effect of patient movement with longer dynamic scan times [8]. However, various image registration techniques, specific to DCE, are being developed which may go some way to mitigating these effects [30, 31]. Such effects could be investigated using the current phantom system, using techniques similar to previous phantom studies where motion was simulated [32].

The phantom used in the present study was designed to be anthropomorphic in both size and complexity, mimicking the conditions associated with abdominal patient imaging; as such, the protocols tested herein faced the same challenges, such as B_1 and B_0 inhomogeneity, inadequate spoiling, and off-resonance effects, all of which may have contributed to the errors in the MR measurements. Although some of these homogeneity issues were compensated for in the present study, future work using this quantitative phantom-based approach will probe these effects in more detail. It is worth noting that in the present study, $T_{res} < 8.1$ s were achieved using the commonly used and easily implementable technique of parallel imaging, which caused an inevitable reduction in both SNRs. SNR values have been shown to exert an influence of the precision of derived PK parameters [28], and while no consistent pattern of decreased precision with SNR was noted in the current study, nevertheless, it would be interesting to investigate this in more detail; this is the focus on on-going work with the model phantom system. Furthermore, the use of more complex PK models, which offer the potential to reveal additional (patho-)physiological information yet have an increased sensitivity to SNR [28] and T_{res} [14], are also the focus of on-going work.

Conclusion

This phantom study demonstrated the critical dependence of the accuracy of model-free phenomenological and pharmacokinetic parameters derived from DCE-MRI data on the T_{res} and AD used in the acquisition. K^{trans} errors were below 14% for acquisitions with $T_{res} \leq 8.1$ s and AD ≥ 360 s, but increased dramatically for longer T_{res} and shorter AD values. v_e errors were below 12% for acquisitions with $T_{res} \leq 16.3$ s and AD ≥ 360 s, and again increased dramatically outside of this range. No major gain in K^{trans}, v_e, and *wash-in* parameters measurement accuracy was found from the use of AD ≥ 360 s, at $T_{res} \leq 8.1$ s (all measurement errors were <15%). The use of quantitative, phantom-based approaches, such as the one described in this study, to access the accuracy and precision of DCE-MRI techniques, offers the prospect of standardising DCE acquisition protocols for the prostate and beyond, and, ultimately, a wider acceptance of the technique for use in routine clinical examinations.

Authors' contribution Knight: Protocol/project development, data collection or management, data analysis. Browne: Protocol/project development. Meaney: Data collection or management. Fagan: Protocol/project development, data collection or management, data analysis.

Compliance with ethical standards

Conflict of interest The authors declare that they have no conflicts of interest. For this type of study, formal consent is not required.

Ethical standards This article does not contain any studies with human participants or animals performed by any of the authors.

Informed consent For this type of study formal consent is not required.

References

1. Noworolski SM, Vigneron DB, Chen AP, Kurhanewicz J (2008) Dynamic contrast-enhanced MRI and MR diffusion imaging to distinguish between glandular and stromal prostatic tissues. Magn Reson Imaging 26:1071–1080
2. Vos EK, Litjens GJ, Kobus T, Hambrock T, Hulsbergen-van de Kaa CA, Barentsz JO, Huisman HJ, Scheenen TW (2013) Assessment of prostate cancer aggressiveness using dynamic contrast-enhanced magnetic resonance imaging at 3 T. Eur Urol 64:448–455
3. Schlemmer HP, Merkle J, Grobholz R, Jaeger T, Michel MS, Werner A, Rabe J, van Kaick G (2004) Can pre-operative contrast-enhanced dynamic MR imaging for prostate cancer predict microvessel density in prostatectomy specimens? Eur Radiol 14:309–317
4. Futterer JJ, Heijmink SW, Scheenen TW, Veltman J, Huisman HJ, Vos P, Hulsbergen-Van de Kaa CA, Witjes JA, Krabbe PF, Heerschap A, Barentsz JO (2006) Prostate cancer localization with dynamic contrast-enhanced MR imaging and proton MR spectroscopic imaging. Radiology 241:449–458
5. Hara N, Okuizumi M, Koike H, Kawaguchi M, Bilim V (2005) Dynamic contrast-enhanced magnetic resonance imaging (DCE-MRI) is a useful modality for the precise detection and staging of early prostate cancer. Prostate 62:140–147
6. Chen YJ, Chu WC, Pu YS, Chueh SC, Shun CT, Tseng WY (2012) Washout gradient in dynamic contrast-enhanced MRI is associated with tumor aggressiveness of prostate cancer. J Magn Reson Imaging 36:912–919
7. Sourbron SP, Buckley DL (2013) Classic models for dynamic contrast-enhanced MRI. NMR Biomed 26:1004–1027
8. Verma S, Turkbey B, Muradyan N, Rajesh A, Cornud F, Haider MA, Choyke PL, Harisinghani M (2012) Overview of dynamic contrast-enhanced MRI in prostate cancer diagnosis and management. AJR Am J Roentgenol 198:1277–1288
9. Aerts HJ, Jaspers K, Backes WH (2011) The precision of pharmacokinetic parameters in dynamic contrast-enhanced magnetic resonance imaging: the effect of sampling frequency and duration. Phys Med Biol 56:5665–5678
10. Ginsburg SB, Taimen P, Merisaari H, Vainio P, Bostrom PJ, Aronen HJ, Jambor I, Madabhushi A (2016) Patient-specific pharmacokinetic parameter estimation on dynamic contrast-enhanced MRI of prostate: preliminary evaluation of a novel AIF-free estimation method. J Magn Reson Imaging 44:1405–1414
11. Sullivan DC, Obuchowski NA, Kessler LG, Raunig DL, Gatsonis C, Huang EP, Kondratovich M, McShane LM, Reeves AP, Barboriak DP, Guimaraes AR, Wahl RL (2015) Metrology standards for quantitative imaging biomarkers. Radiology 277:813–825
12. Mehrabian H, Pang I, Chandrana C, Chopra R, Martel AL (2011) Automatic mask generation using independent component analysis in dynamic contrast enhanced-MRI. IEEE Int Symp Biomed Imaging From Nano Macro 1657–1661
13. Rajan S, Herbertson L, Bernardo M, Choyke P (2014) A dialyzer-based flow system for validating dynamic contrast enhanced MR image acquisition. Magn Reson Med 72:41–48
14. Henderson E, Rutt BK, Lee TY (1998) Temporal sampling requirements for the tracer kinetics modeling of breast disease. Magn Reson Imaging 16:1057–1073
15. Othman AE, Falkner F, Martirosian P, Schraml C, Schwentner C, Nickel D, Nikolaou K, Notohamiprodjo M (2016) Optimized fast dynamic contrast-enhanced magnetic resonance imaging of the prostate: effect of sampling duration on pharmacokinetic parameters. Invest Radiol 51:106–112
16. Othman AE, Falkner F, Weiss J, Kruck S, Grimm R, Martirosian P, Nikolaou K, Notohamiprodjo M (2016) Effect of temporal resolution on diagnostic performance of dynamic contrast-enhanced magnetic resonance imaging of the prostate. Invest Radiol 51:290–296
17. Rosenkrantz AB, Geppert C, Grimm R, Block TK, Glielmi C, Feng L, Otazo R, Ream JM, Romolo MM, Taneja SS, Sodickson DK, Chandarana H (2015) Dynamic contrast-enhanced MRI of the prostate with high spatiotemporal resolution using compressed sensing, parallel imaging, and continuous golden-angle radial sampling: preliminary experience. J Magn Reson Imaging 41:1365–1373
18. Barrett T, Gill AB, Kataoka MY, Priest AN, Joubert I, McLean MA, Graves MJ, Stearn S, Lomas DJ, Griffiths JR, Neal D,

Gnanapragasam VJ, Sala E (2012) DCE and DW MRI in monitoring response to androgen deprivation therapy in patients with prostate cancer: a feasibility study. Magn Reson Med 67:778–785

19. Haq NF, Kozlowski P, Jones EC, Chang SD, Goldenberg SL, Moradi M (2015) A data-driven approach to prostate cancer detection from dynamic contrast enhanced MRI. Comput Med Imaging Graph 41:37–45

20. Villers A, Puech P, Mouton D, Leroy X, Ballereau C, Lemaitre L (2006) Dynamic contrast enhanced, pelvic phased array magnetic resonance imaging of localized prostate cancer for predicting tumor volume: correlation with radical prostatectomy findings. J Urol 176:2432–2437

21. Knight SP, Browne JE, Meaney JF, Smith DS, Fagan AJ (2016) A novel anthropomorphic flow phantom for the quantitative evaluation of prostate DCE-MRI acquisition techniques. Phys Med Biol 61:7466–7483

22. Tofts PS, Brix G, Buckley DL, Evelhoch JL, Henderson E, Knopp MV, Larsson HB, Lee TY, Mayr NA, Parker GJ, Port RE, Taylor J, Weisskoff RM (1999) Estimating kinetic parameters from dynamic contrast-enhanced T(1)-weighted MRI of a diffusable tracer: standardized quantities and symbols. J Magn Reson Imaging 10:223–232

23. Parker GJ, Roberts C, Macdonald A, Buonaccorsi GA, Cheung S, Buckley DL, Jackson A, Watson Y, Davies K, Jayson GC (2006) Experimentally-derived functional form for a population-averaged high-temporal-resolution arterial input function for dynamic contrast-enhanced MRI. Magn Reson Med 56:993–1000

24. Sandler K, Patel M, Lynne C, Parekh DJ, Punnen S, Jorda M, Casillas J, Pollack A, Stoyanova R (2015) Multiparametric-MRI and targeted biopsies in the management of prostate cancer patients on active surveillance. Front Oncol 5:4

25. Lin LI (1989) A concordance correlation coefficient to evaluate reproducibility. Biometrics 45:255–268

26. Smith DS, Li X, Arlinghaus LR, Yankeelov TE, Welch EB (2015) DCEMRI.jl: a fast, validated, open source toolkit for dynamic contrast enhanced MRI analysis. PeerJ 3:e909

27. Dietrich O, Raya JG, Reeder SB, Reiser MF, Schoenberg SO (2007) Measurement of signal-to-noise ratios in MR images: influence of multichannel coils, parallel imaging, and reconstruction filters. J Magn Reson Imaging 26:375–385

28. Li X, Huang W, Rooney WD (2012) Signal-to-noise ratio, contrast-to-noise ratio and pharmacokinetic modeling considerations in dynamic contrast-enhanced magnetic resonance imaging. Magn Reson Imaging 30:1313–1322

29. Kim JK, Hong SS, Choi YJ, Park SH, Ahn H, Kim CS, Cho KS (2005) Wash-in rate on the basis of dynamic contrast-enhanced MRI: usefulness for prostate cancer detection and localization. J Magn Reson Imaging 22:639–646

30. Chen X, Salerno M, Yang Y, Epstein FH (2014) Motion-compensated compressed sensing for dynamic contrast-enhanced MRI using regional spatiotemporal sparsity and region tracking: block low-rank sparsity with motion-guidance (BLOSM). Magn Reson Med 72:1028–1038

31. Melbourne A, Hipwell J, Modat M, Mertzanidou T, Huisman H, Ourselin S, Hawkes DJ (2011) The effect of motion correction on pharmacokinetic parameter estimation in dynamic-contrast-enhanced MRI. Phys Med Biol 56:7693–7708

32. Stone AJ, Browne JE, Lennon B, Meaney JF, Fagan AJ (2012) Effect of motion on the ADC quantification accuracy of whole-body DWIBS. Magn Reson Mater Phy 25:263–266